JACS Au
AN OPEN ACCESS JOURNAL OF THE AMERICAN CHEMICAL SOCIETY

pubs.acs.org/jacsau
Article

Theoretical Approach toward a Mild Condition Haber–Bosch Process on the Zeolite Catalyst with Confined Dual Active Sites

Chunli Liu,[‖] Gaomou Xu,[‖] and Tao Wang*

Cite This: JACS Au 2023, 3, 3374–3380
Read Online

ACCESS | Metrics & More | Article Recommendations | Supporting Information

ABSTRACT: The Haber–Bosch (H–B) process is today's dominant technology for ammonia production, but achieving a mild reaction condition is still challenging. Herein, we combined density functional theory (DFT) calculations and microkinetic modeling (MKM) to demonstrate the feasibility of conducting the H–B process under ambient conditions on a zeolite catalyst with confined dual active sites. Our designed dual Mo(II) cation-anchored ferrierite [2Mo$^{(II)}$-FER] catalyst shows an energy barrier of only 0.58 eV for N≡N bond breaking due to the enhanced π-back-donation. Meanwhile, the three hydrogen sources (BH, FMH, and NMH) within 2Mo$^{(II)}$-FER greatly enrich the hydrogenation mechanisms of NH_x species, resulting in barriers of <1.1 eV for NH_x (x = 0–2) hydrogenations. This dual-site catalyst properly decouples the N_2 dissociation and NH_x hydrogenation steps, which elegantly circumvents the linear scaling relation between the N_2 dissociation barrier and the nitrogen binding energy. It is worth noting that our MKM results show 4 orders of magnitude higher reaction rates on 2Mo$^{(II)}$-FER than the stepped sites of the FCC Ru catalyst at low temperatures, paving a solid basis to conduct the H–B process at low temperatures. We believe that our strategy will provide crucial guidance for synthesizing state-of-the-art zeolite catalysts to achieve the near-ambient condition H–B process and other chemical reactions in heterogeneous catalysis.

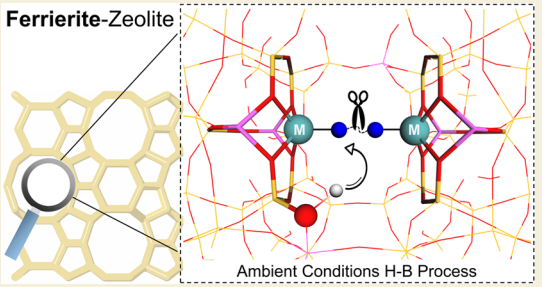

KEYWORDS: *Haber–Bosch, zeolite, ambient condition, confined dual-site, DFT*

INTRODUCTION

Ammonia (NH_3) is one of the chemicals most important to human beings, with wide applications in agriculture, industry, and carbon-free fuels.[1−3] Currently, the century-old Haber–Bosch (H–B) process is still the dominant technology for NH_3 synthesis. Meanwhile, the H–B process has been an ideal model reaction for the fundamental understanding of heterogeneous catalysis in the gas–solid interface.[4] Gerhard Ertl was awarded the 2007 Nobel Prize in chemistry for his studies of chemical processes on solid surfaces, while the identification of N_2 dissociation as the rate-determining step (RDS) of the H–B process on the iron-based catalyst was one of his most significant achievements.[5,6] Unfortunately, a high temperature (300∼500 °C) is needed to drive this RDS owing to the extreme inertness of the N≡N bond (941 kJ/mol), but will inevitably suppress the equilibrium conversion for NH_3 production due to the exothermic nature of this reaction, which clearly necessitates a high pressure (150∼200 bar) to guarantee a reasonable conversion.[7] Such harsh reaction conditions combined with the utilization of gray hydrogen result in high energy consumption and CO_2 emission, which makes the development of ambient condition H–B process imminent.[8] Even worse, the well-established scaling relations between the N_2 dissociation barrier and atomic N binding energy among transition metals set formidable challenges to designing optimal catalysts capable of breaking the N≡N bond with a low energy barrier and simultaneously maintaining a weak N binding strength to avoid being limited by the hydrogenation steps.[9]

Indeed, scientists have spared no efforts to develop strategies to achieve ambient H–B processes such as alloying,[10] LiH-mediation,[11] strain engineering,[12] defect engineering,[13] and magnetic steering.[14] Our recent work theoretically proposed an ideal model catalyst with confined dual sites to achieve a mild condition H–B process, where the inert N≡N bond could be easily activated via the enhanced π-back-donation (Figure 1A) from the two-sided Co metals and weak binding strength of NH_x species is also reserved.[15] However, the design of more realistic catalysts with high synthetic feasibility in the laboratory represents a major challenge to extending the application of our proposed principle. To this end, we theoretically evaluated a large number of materials, where the zeolites with uniform microporous structures and superior

Received: September 17, 2023
Revised: October 27, 2023
Accepted: October 27, 2023
Published: November 7, 2023

https://doi.org/10.1021/jacsau.3c00546
JACS Au 2023, 3, 3374–3380

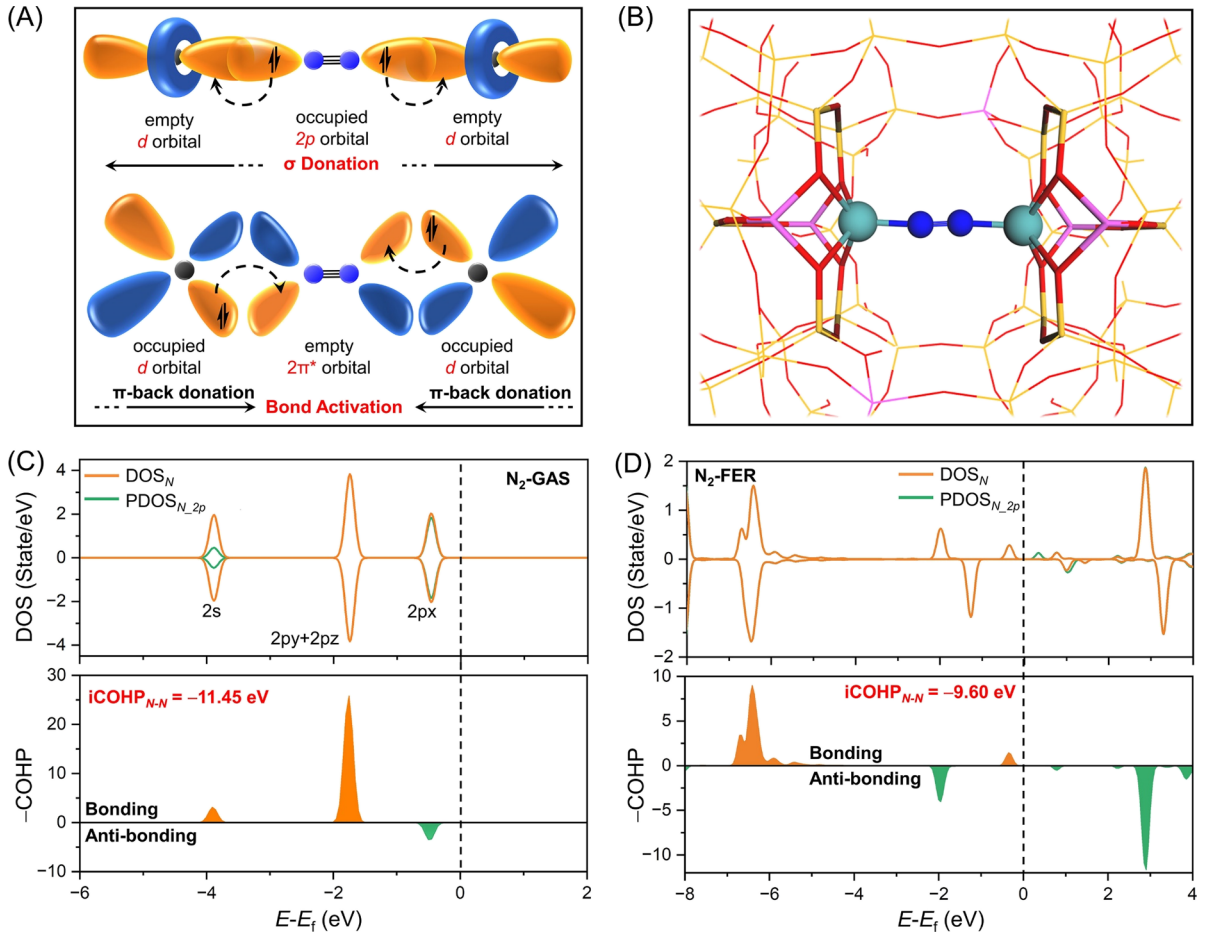

Figure 1. (A) Schematic diagram of enhanced π back-donation; (B) dual metal active sites anchored in ferrierite zeolite catalyst, where blue and green spheres denote nitrogen and metal atoms, while the yellow, red, and purple sticks denote the silicon, oxygen, and aluminum in the zeolite; DOS and COHP structure of free (C) and adsorbed N_2 (D) molecule (the Fermi energy level is set to zero as the energy reference).

thermal stability were proposed as the superior frameworks to properly anchor the dual active sites (Figure 1B) and achieve a milder condition H−B process. Unfortunately, there are very limited studies of ammonia synthesis within zeolite partially due to the acidic nature, which is a double-edged sword to ammonia synthesis, i.e., the Brønsted acid works as an ideal hydrogen source for hydrogenation but also preferably forms NH_4^+ with NH_3, resulting in the difficulty in product desorption.[16] Cisneros et al. reported the study of the ammonia synthesis on Ru metal within potassium-promoted zeolite,[17] while subsequent research focused on the replacement of alkaline metals with alkaline earth metals to further promote the activity of Ru-supported zeolite catalysts.[18−22] Qiu et al. reported that the Ru single atom confined in the siliceous zeolite showed surprising ammonia synthesis activity compared to the conventional Ru catalyst.[23] Additionally, MoN_x confined in zeolite also shows much better activity for ammonia synthesis than bulk Mo_2N, but the active site and mechanism are unclear.[24,25] Interestingly, Skelnak et al. confined binuclear cationic Fe(II) centers within zeolites and found their superior activities in N_2O decomposition and dioxygen splitting.[26−28] All the abovementioned information laid a good basis for achieving effective N_2 activation and ammonia synthesis by using zeolite with a confined metal dual-site in the framework.

In this work, to effectively achieve simultaneous bonding of N_2 molecules on both sides, the ferrierite (FER) zeolite with the largest sphere diameter of 6.31 Å[29] is chosen as the framework to anchor dual metal active sites for effective N≡N activation, as shown in Figure 1B. By means of density functional theory (DFT) calculations, we systematically simulate the reaction mechanism of ammonia synthesis on the dual Mo(II) sites anchored FER [$2Mo^{(II)}$-FER], while the mean-field microkinetic modeling (MKM) shows 4 orders of magnitude higher turnover frequency (TOF) for NH_3 than the step (211) surface of the FCC Ru metal under the same reaction condition. We elegantly demonstrate the feasibility of using zeolite with confined dual active sites and well-controlled acidity to catalyze NH_3 synthesis, laying a good basis for achieving a mild H−B process. Meanwhile, the active sites for N_2 activation and H binding are decoupled due to the existence of Brønsted acid in zeolite, which facilitates the independent optimization of the N_2 activation and NH_x hydrogenation steps and elegantly circumvents the linear scaling relation in ammonia synthesis. We believe that our proposed confined dual active sites within zeolite hold great potential for practical applications in mild-condition reactions.

RESULTS AND DISCUSSION

N_2 Activation on the FER Zeolite with Confined Dual-Site [$2M^{(II)}$-FER]

The N_2 activation has been proven to be the rate-determining step for the H−B process.[5] Unfortunately, the high N≡N

https://doi.org/10.1021/jacsau.3c00546
JACS Au 2023, 3, 3374−3380

triple bond energy (941 kJ/mol), as well as the large energy gap between the highest occupied molecular orbital (HOMO, −15.6 eV) and the lowest unoccupied molecular orbital (LUMO, 7.3 eV), made effective N_2 activation and electron transfer very challenging.[30] Based on the molecular orbital theory in Figure 1A, our proposed dual-site strategy provides an ideal route to effectively activate N_2 as long as active sites have both suitable numbers of free electrons and available empty orbitals.

Taking the 2Mo$^{(II)}$-FER as an example shown in Figure 1B (other metals are shown in Table S1), two Mo(II) cations with a distance of 5.62 Å possess the high-spin $4d^4\uparrow$ electron configurations.[28] The N_2 molecule simultaneously bonds with two Mo(II) cations and forms a bridge configuration [Mo(II)−(N═N)−Mo(II)] with an adsorption energy of −1.53 eV, while the N≡N bond is prolonged from 1.11 Å in the gas phase to 1.21 Å. The calculated N−N stretching vibration frequency of 1701 cm^{-1} strongly confirms the activation of stable N≡N bonding (2436 cm^{-1} for the free N_2 molecule).

To understand the underlying electronic structures of the configuration, we further analyzed the density of state (DOS) associated with the crystal orbital Hamilton population (COHP)[31] For the free N_2 molecule in Figure 1C, the bonding contributions to the N≡N bond mainly come from the 2π orbital, while the empty π^* orbital displays an obvious antibonding state according to the molecular orbital surface (Figure S7). The iCOHP value is equal to −11.45 eV. For the adsorbed N_2 on FER zeolite in Figure 1D, the N_2-2p orbitals significantly lowered the energy level owing to the hybrid with the metal 4*d* orbitals, making them much easier to accept the back-donated electrons from Mo(II) cations to achieve effective N≡N bond activation. The iCOHP value for the [Mo(II)−(N═N)−Mo(II)] bond shifts to −9.60 eV, which clearly indicates the activated N≡N bonds.

Ammonia Synthesis Reaction Mechanism on the 2Mo$^{(II)}$-FER

For the typical H−B process, effective activation and cleavage of the N≡N bond produce 2N on the active sites, followed by subsequent hydrogenation to NH_3, while NH_3 desorption is the final step. Figure 2A shows the detailed reaction mechanism of ammonia synthesis on the 2Mo$^{(II)}$-FER, while the potential energy diagram of the whole reaction network is plotted in Figure 2B. For the highly activated N_2 molecule within the 2Mo$^{(II)}$-FER catalyst [Mo(II)−(N═N)−Mo(II)], the N≡N bond breaking only needs an energy barrier of 0.58 eV and results in two Mo(II)-N intermediates, which has a binding energy of −1.77 eV and a Mo(II)-N bond length of 1.67 Å (detailed in Figure S2).

Different from the traditional metal-based catalysts, the newly designed 2Mo$^{(II)}$-FER has three different hydrogen sources shown in Figure 2B, i.e., the BH within the zeolite, the H near the N on the Mo(II) site (NMH), and the H far from the N on the other Mo(II) site (FMH), which greatly enrich the hydrogenation mechanisms. We considered three different pathways from three H sources for the first hydrogenation step to the Mo(II)−NH intermediate. For the BH pathway, the production of NH has an energy barrier of 1.34 eV. At the transition state (TS), the bond lengths of Mo(II)−N and N-BH are 1.71 and 1.26 Å, respectively. For the NMH pathway, the NMH and N atom coadsorbed on the same Mo(II) site, and the energy barrier for N + H → NH is 1.46 eV, which is

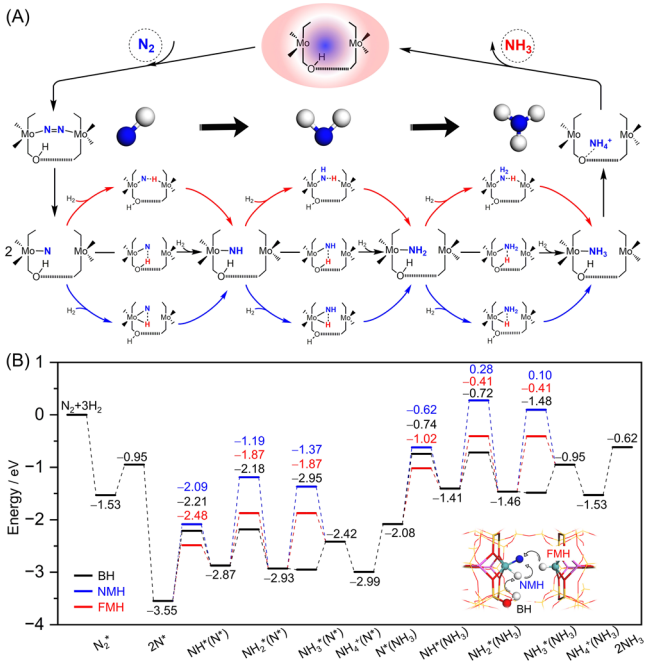

Figure 2. Reaction mechanism of the H−B process with different H sources (A) and potential energy profiles on the designed 2Mo$^{(II)}$-FER catalyst (B) at 0 K with zero-point energy corrections.

slightly higher than that of the BH pathway. At the TS, the distance between N and NMH is 1.43 Å. For the FMH pathway, the H atom binds on the opposite Mo(II) site, which increases the probability of collision to reaction with each other, and this hydrogenation step has an energy barrier of only 1.06 eV with the FMH−N bond length of 1.30 Å. It is worth noting that the FMH pathway provides an ideal structure for the overlap of the s orbital of H with the frontier orbital of the N, resulting in the low energy barrier (detailed structures of the TS are shown in Figures S8−S10).

For further hydrogenation steps, three H sources result in quite different energy barriers. For the BH pathway, the energy barriers for NH to NH_2 and NH_2 to NH_3 steps are only 0.69 eV and ∼0 eV, respectively, while those of NMH (1.68 and 1.56 eV) and FMH pathways (1.00 and 1.06 eV) are much higher (detailed information for TSs is provided in Table S5). Finally, the desorption of NH_3 from the Mo(II) site is endothermic by 0.34 eV. However, the desorption mechanism of NH_3 from zeolite is different from the solid catalysts due to the existence of the BH site. Instead of a direct desorption to the gas phase, the produced ammonia tends to bind with the BH site and forms the stable NH_4^+ intermediate via the acid−base neutralization reaction (detailed structure is shown in Figure S11). Therefore, the actual desorption process starts from NH_4^+ to gaseous NH_3 and is accompanied by the regeneration of BH. This process is endothermic by 0.91 eV on the 2Mo$^{(II)}$-FER.

Clearly, the three different H sources within the newly designed 2Mo$^{(II)}$-FER catalyst provide ample space to optimize the hydrogenation steps during the H−B process. As shown in Figure 3, pathways (1)−(3), the FMH pathway has a very low energy barrier (1.06 eV) for the N hydrogenation to NH, while the BH pathway has very low energy barriers for NH (0.69 eV) and NH_2 (∼0 eV) hydrogenations. Ideally, ammonia synthesis will take the most favorable elementary steps to produce NH_3. Therefore, the hybrid pathway with very low energy barriers

https://doi.org/10.1021/jacsau.3c00546
JACS Au 2023, 3, 3374−3380

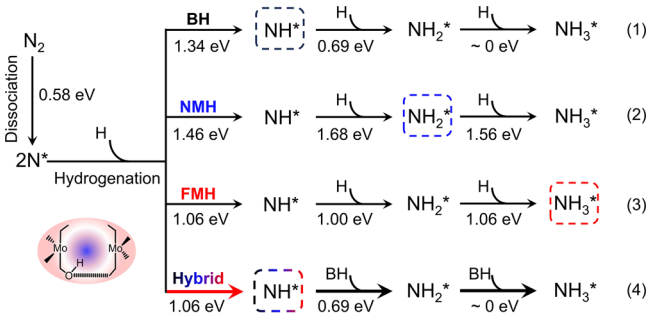

Figure 3. Reaction pathways of different H sources within the $2Mo^{(II)}$-FER.

for each elementary step shown in pathway (4) represents the best scenario to conduct ammonia synthesis within the $2Mo^{(II)}$-FER catalyst, which holds great potential to achieve a mild condition H−B process.

Reaction Rates of Ammonia Synthesis on the $2Mo^{(II)}$-FER and Ru Catalysts

To further evaluate the reaction rate of the $2Mo^{(II)}$-FER catalyst in ammonia synthesis, we established a mean-field MKM to calculate the turnover frequency of NH_3 production (TOF_{NH3}) under different conditions. To have a convenient comparison, we also chose the stepped (211) surface of FCC Ru as the benchmark, which has been widely regarded as the most active metal for ammonia synthesis. Figure 4A,B plots the TOF_{NH3} as a function of temperature and total pressure on the $2Mo^{(II)}$-FER and Ru(211) surfaces, where our newly designed catalyst shows a much higher TOF for ammonia synthesis under the same reaction condition. More specifically, at a pressure of 100 bar (N_2/H_2 = 1/3) shown in Figure 4C, the TOF of NH_3 production on the $2Mo^{(II)}$-FER catalyst (4.86×10^{-2} s^{-1}) is 4 orders of magnitude higher than the Ru(211) surface (2.60×10^{-6} s^{-1}) at 500 K. Likewise, at the typical temperature of 673 K for the H−B process in Figure 4D, $2Mo^{(II)}$-FER shows superior activity of 1.49 s^{-1}, which is also 4 orders of magnitude higher than Ru (211) surface (1.46×10^{-4} s^{-1}) under atmospheric pressure of 1 bar. All the simulated results mentioned above clearly indicate the high potential to achieve a mild condition H−B process with our newly designed zeolite catalyst confined with dual Mo(II) active sites.

CONCLUSIONS

In summary, we illustrate the high feasibility of achieving a mild condition Haber−Bosch process on the ferrierite zeolite catalyst with confined dual Mo(II) active sites by using density functional theory calculations and microkinetic modeling, which has not yet been reported in previous research on heterogeneous catalysis. Our proposed new strategy to enhance the π-back-donation to the π^* orbital of the N_2 molecule via the dual active sites successfully achieves a facile breaking of the N≡N bond with an energy barrier of only 0.58 eV. Notably, the existence of BH and the dual active sites within zeolite greatly enrich the hydrogenation mechanisms on the $2Mo^{(II)}$-FER catalyst, resulting in BH, NMH, and FMH hydrogenation pathways with quite different energy barriers. This scenario clearly facilitates the decoupling of the N_2 dissociation and NH_x hydrogenation steps because N_2 and H could in principle bind on different active sites within the $2Mo^{(II)}$-FER catalyst, which elegantly circumvents the linear scaling relation between the N_2 dissociation energy barrier and nitrogen binding energy. As a result, the hybrid hydrogenation pathways with three different hydrogen sources greatly decrease the energy barriers of all elementary steps in ammonia synthesis, i.e., the $N_2 \xrightarrow{\text{Diss.}} N \xrightarrow{\text{FMH}} NH \xrightarrow{\text{BH}} NH_2 \xrightarrow{\text{BH}} NH_3$ pathway has a maximum barrier of only 1.06 eV. Our mean-

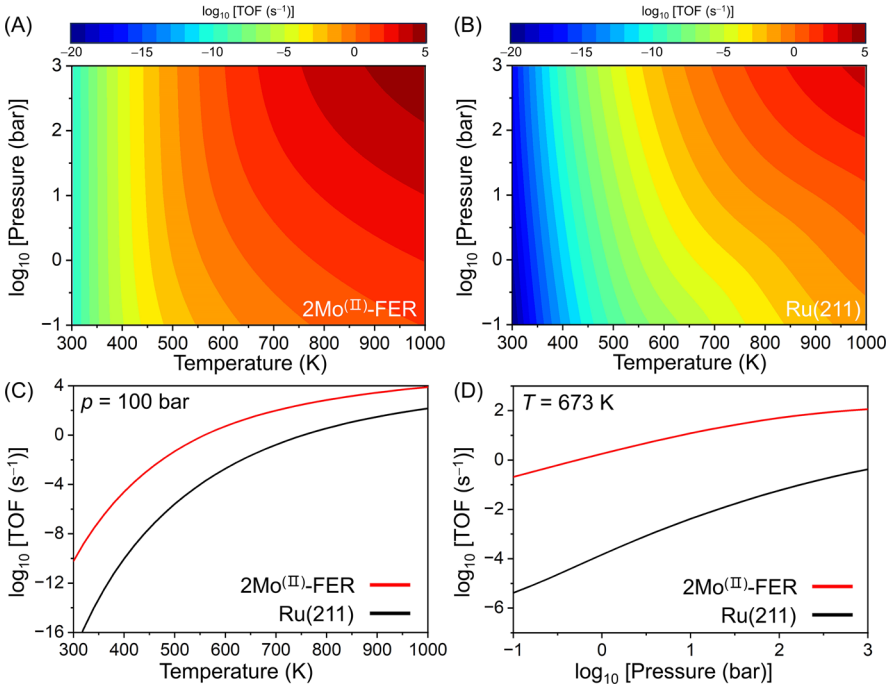

Figure 4. Calculated TOF of NH_3 production as a function of temperatures and total pressures at N_2/H_2 = 1/3 on the $2Mo^{(II)}$-FER (A) and stepped FCC Ru(211) surface. (B) as well as the temperature dependence at 100 bar (C) and pressure dependence at 673 K (D) with N_2/H_2 = 1/3. The data on Ru(211) are taken from our own work in ref 15, Copyright 2021 National Academy of Sciences.

https://doi.org/10.1021/jacsau.3c00546
JACS Au 2023, 3, 3374−3380

field microkinetic modeling identified about 4 orders of magnitude higher TOF of NH_3 on the $2Mo^{(II)}$-FER catalyst than the most active stepped Ru catalyst under the same mild reaction conditions. This work provides solid theoretical evidence to achieve a mild Haber−Bosch process using the zeolite catalyst with dual active sites confined in cages. We believe that our proposed $2Mo^{(II)}$-FER catalyst has a very high feasibility to be synthesized experimentally, leading to a robust theoretical basis for the design of the state-of-the-art catalysts to achieve a high reaction rate of ammonia synthesis under ambient conditions.

METHODS

All the periodic plane-wave-based DFT calculations were performed using the Vienna ab initio simulation package[32] within generalized gradient approximation.[33] The exchange-correlation contribution to the electronic energy was described by the BEEF-vdW functional,[34] which has been demonstrated to be adequate to quantitatively describe the van der Waals interaction between molecules and zeolite pores[35] as well as reaction kinetics.[36] The energy cutoff for the plane wave was set to be 500 eV, and the convergence criteria of total energy and forces were 10^{-4} and 0.05 eV/Å, respectively (the data of various parameter settings are shown in Table S6). Brillouin zone sampling was restricted to the Γ point.[37] All of the optimizations are performed with spin polarization. For both the active site and all the intermediates, additional calculations with a fixed spin state were conducted to identify the most stable spin state, and all of the related data are summarized in Table S4. The transition state (TS) structure was located using the climbing-image nudged elastic band method (CI-NEB).[38] Frequency analysis was carried out to determine zero-point energy (ZPE) and to characterize the nature of the optimized stationary points, where the right TS has only one imaginary frequency. All reported energetic data in the potential energy diagram include the corrections of ZPEs, while the thermodynamic corrections to all of the species were included in our mean-field microkinetic modeling.

To discuss the reaction under realistic conditions, the CatMAP code[39] was applied to solve the differential equations in our mean-field microkinetic modeling and calculate the TOF of ammonia synthesis under different reaction conditions (details are shown in Supporting Information).

In our calculation, the optimized lattice parameters of the all-silica FER are a = 19.107 Å, b = 14.300 Å, c = 7.564 Å, which agrees very well with the data from the IZA database (a = 19.018 Å, b = 14.303 Å, c = 7.541 Å)[29] and indicates the sufficient accuracy of BEEF-vdW functional in modeling our designed $2Mo^{(II)}$-FER catalyst. As shown in Figure 1B, the model has P1 symmetry and features a supercell composed of two unit cells along the c dimension. The model contains four Al/Si substitutions forming two α[26,27] sites with the four Al atoms located in the T3 site[40] of the adjacent six rings facing each other across the 10-ring channel, and two metal cations with a valence of two [M(II)] were introduced to balance the charge for neutrality (detailed information is provided in Figure S1). Each M(II) cation coordinated with four neighboring oxygen atoms of the zeolite framework to form square pyramidal configurations. Additionally, ab initio molecular dynamics simulations within the canonical ensemble (NVT) were employed for 5 ps with a time step of 1 fs at 1000 K to evaluate the dynamic stability of the designed catalyst, and all the details are shown in Figure S3 and Table S3. The structure of the designed catalyst with and without the intermediate remained stable without bond breaking. For the hydrogenation steps, according to the locations, there are three possible hydrogen sources (detailed in Figure S4): Brønsted hydrogen (BH), far metal hydrogen (FMH), and near metal hydrogen (NMH). The BH serves as the charge compensator to neutralize the introduced negative charge during the Si(IV)/Al(III) substitution, which is the natural property of zeolite in the preparation process. Based on our simulations, H_2 could undergo dissociation on both Mo(II) and Al−O sites within the zeolite, while that on Mo(II) sites has a relatively low energy barrier and forms MH and BH on the active sites. The related structures of the H_2 dissociation process on Mo(II) sites are detailed in Figure S5.

ASSOCIATED CONTENT

Supporting Information

The Supporting Information is available free of charge at https://pubs.acs.org/doi/10.1021/jacsau.3c00546.

Possible structures containing Al/Si substitutions in the different T sites, comparison of dissociation energy barrier of the N≡N bond between $2Mo^{(II)}$ and $2Ru^{(II)}$ active sites, AIMD simulation results, model and locations for the different hydrogen sources, detailed structure of H_2 dissociated on $2Mo^{(II)}$-FER, molecular orbital surface, structure parameters and energies, formation energy, average bond lengths, relative energies, structure parameters of transition states, and comparison of different parameters setting for the total energies (PDF)

AUTHOR INFORMATION

Corresponding Author

Tao Wang − *Center of Artificial Photosynthesis for Solar Fuels and Department of Chemistry, School of Science and Research Center for Industries of the Future, Westlake University, Hangzhou 310030 Zhejiang Province, China; Institute of Natural Sciences, Westlake Institute for Advanced Study, Hangzhou 310024 Zhejiang Province, China; Division of Solar Energy Conversion and Catalysis at Westlake University, Zhejiang Baima Lake Laboratory, Hangzhou 310000 Zhejiang Province, China;* orcid.org/0000-0003-4451-2721; Email: twang@westlake.edu.cn

Authors

Chunli Liu − *Center of Artificial Photosynthesis for Solar Fuels and Department of Chemistry, School of Science and Research Center for Industries of the Future, Westlake University, Hangzhou 310030 Zhejiang Province, China; Institute of Natural Sciences, Westlake Institute for Advanced Study, Hangzhou 310024 Zhejiang Province, China*

Gaomou Xu − *Center of Artificial Photosynthesis for Solar Fuels and Department of Chemistry, School of Science and Research Center for Industries of the Future, Westlake University, Hangzhou 310030 Zhejiang Province, China; Institute of Natural Sciences, Westlake Institute for Advanced Study, Hangzhou 310024 Zhejiang Province, China*

Complete contact information is available at: https://pubs.acs.org/10.1021/jacsau.3c00546

Author Contributions

‖C.L. and G.X. contributed equally to this work. T.W. conceptualized the ideas for this study; C.L. conducted DFT calculations, G.X. contributed to microkinetics simulations; all authors were involved in writing and editing the paper. CRediT: **Chunli Liu** data curation, formal analysis, investigation, writing-original draft; **Gaomou Xu** data curation, formal analysis, investigation, methodology, resources; **Tao Wang** conceptualization, formal analysis, funding acquisition, investigation, methodology, project administration, resources, supervision, validation, writing-review & editing.

https://doi.org/10.1021/jacsau.3c00546
JACS Au 2023, 3, 3374−3380

Notes

The authors declare no competing financial interest.

■ ACKNOWLEDGMENTS

This work was supported by the National Natural Science Foundation of China (22273076) and the National Key Research and Development Program of China (2022YFA0911900); T.W. thanks the start-up packages from Westlake University and the Kunpeng research fund from Zhejiang Province. We thank the Research Center for Industries of the Future (RCIF) at Westlake University for supporting this work. We thank Westlake University HPC Center for computation support. We also thank Mr. Yonghua Liu for his support regarding the microkinetic modeling. This work is dedicated to Prof. Haijun Jiao on the occasion of his 60th birthday.

■ REFERENCES

(1) Foster, S. L.; Bakovic, S. I. P.; Duda, R. D.; Maheshwari, S.; Milton, R. D.; Minteer, S. D.; Janik, M. J.; Renner, J. N.; Greenlee, L. F. Catalysts for Nitrogen Reduction to Ammonia. *Nat. Catal.* **2018**, *1* (7), 490−500.

(2) MacFarlane, D. R.; Cherepanov, P. V.; Choi, J.; Suryanto, B. H. R.; Hodgetts, R. Y.; Bakker, J. M.; Ferrero Vallana, F. M.; Simonov, A. N. A Roadmap to the Ammonia Economy. *Joule* **2020**, *4* (6), 1186−1205.

(3) Chen, Z.; Liu, C.; Sun, L.; Wang, T. Progress of Experimental and Computational Catalyst Design for Electrochemical Nitrogen Fixation. *ACS Catal.* **2022**, *12* (15), 8936−8975.

(4) Ertl, G. Reactions at Surfaces: from Atoms to Complexity (Nobel Lecture). *Angew. Chem., Int. Ed. Engl.* **2008**, *47* (19), 3524−3535.

(5) Ertl, G. Primary Steps in Catalytic Synthesis of Ammonia. *J. Vac. Sci. Technol. A* **1983**, *1* (2), 1247−1253.

(6) Bowker, M. The 2007 Nobel Prize in Chemistry for Surface Chemistry: Understanding Nanoscale Phenomena at Surfaces. *ACS Nano* **2007**, *1* (4), 253−257.

(7) Meng, S.-L.; Li, X.-B.; Tung, C.-H.; Wu, L.-Z. Nitrogenase Inspired Artificial Photosynthetic Nitrogen Fixation. *Chem* **2021**, *7* (6), 1431−1450.

(8) Klerke, A.; Christensen, C. H.; Nørskov, J. K.; Vegge, T. Ammonia for Hydrogen Storage: Challenges and Opportunities. *J. Mater. Chem.* **2008**, *18* (20), 2304−2310.

(9) Medford, A. J.; Vojvodic, A.; Hummelshøj, J. S.; Voss, J.; Abild-Pedersen, F.; Studt, F.; Bligaard, T.; Nilsson, A.; Nørskov, J. K. From the Sabatier Principle to a Predictive Theory of Transition-metal Heterogeneous Catalysis. *J. Catal.* **2015**, *328*, 36−42.

(10) Jacobsen, C. J. H.; Dahl, S.; Clausen, B. S.; Bahn, S.; Logadottir, A.; Nørskov, J. K. Catalyst Design by Interpolation in the Periodic Table: Bimetallic Ammonia Synthesis Catalysts. *J. Am. Chem. Soc.* **2001**, *123*, 8404−8405.

(11) Wang, P.; Chang, F.; Gao, W.; Guo, J.; Wu, G.; He, T.; Chen, P. Breaking Scaling Relations to Achieve Low-temperature Ammonia Synthesis through LiH-mediated Nitrogen Transfer and Hydrogenation. *Nat. Chem.* **2017**, *9* (1), 64−70.

(12) Khorshidi, A.; Violet, J.; Hashemi, J.; Peterson, A. A. How Strain Can Break the Scaling Relations of Catalysis. *Nat. Catal.* **2018**, *1* (4), 263−268.

(13) Ye, T. N.; Park, S. W.; Lu, Y.; Li, J.; Sasase, M.; Kitano, M.; Tada, T.; Hosono, H. Vacancy-enabled N_2 Activation for Ammonia Synthesis on an Ni-loaded Catalyst. *Nature* **2020**, *583* (7816), 391−395.

(14) Xu, G.; Cai, C.; Wang, T. Toward Sabatier Optimal for Ammonia Synthesis with Paramagnetic Phase of Ferromagnetic Transition Metal Catalysts. *J. Am. Chem. Soc.* **2022**, *144* (50), 23089−23095.

(15) Wang, T.; Abild-Pedersen, F. Achieving Industrial Ammonia Synthesis Rates at Near-ambient Conditions Through Modified Scaling Relations on a Confined Dual Site. *Proc. Natl. Acad. Sci. U. S. A.* **2021**, *118* (30), No. e2106527118.

(16) Marakatti, V. S.; Gaigneaux, E. M. Recent Advances in Heterogeneous Catalysis for Ammonia Synthesis. *ChemCatChem* **2020**, *12* (23), 5838−5857.

(17) Cisneros, M. D.; Lunsford, J. H. Ammonia-Synthesis with Potassium-Promoted Ruthenium in Zeolite-X. *Abstr. Pap. Am. Chem. Soc.* **1989**, *197*, 124.

(18) Mahdi, W.; Sauerlandt, U.; Wellenbüscher, J.; Schütze, J.; Muhler, M.; Ertl, G.; Schlögl, R. Application of Ru Exchanged Zeolite-Y in Ammonia Synthesis. *Catal. Lett.* **1992**, *14* (3), 339−348.

(19) Fishel, C. T.; Davis, R. J.; Garces, J. M. A Novel Basic Alkaline-earth Zeolite-Supported Ruthenium Catalyst for Ammonia Synthesis. *Chem. Commun.* **1996**, *5*, 649−650.

(20) Fishel, C. T.; Davis, R. J.; Garces, J. M. Ammonia Synthesis Catalyzed by Ruthenium Supported on Basic Zeolites. *J. Catal.* **1996**, *163* (1), 148−157.

(21) McClaine, B. C.; Becue, T.; Lock, C.; Davis, R. J. Kinetic Analysis of Ammonia Synthesis Catalyzed by Barium-Promoted Ruthenium Supported on Zeolite X. *J. Mol. Catal. A: Chem.* **2000**, *163* (1−2), 105−116.

(22) Chen, S.-Y.; Nishi, M.; Chang, A.; Hsiao, W.-C.; Mochizuki, T.; Takagi, H.; Yang, C.-M. Well-ordered Cs−Ru/@ SBA-15 Nanocomposite Materials for Low Pressure Ammonia Synthesis. *Sustainable Energy Fuels* **2020**, *4* (11), 5802−5811.

(23) Qiu, J.-Z.; Hu, J.; Lan, J.; Wang, L.-F.; Fu, G.; Xiao, R.; Ge, B.; Jiang, J. Pure Siliceous Zeolite-Supported Ru Single-Atom Active Sites for Ammonia Synthesis. *Chem. Mater.* **2019**, *31* (22), 9413−9421.

(24) Liu, N.; Nie, L.; Xue, N. H.; Dong, H. H.; Peng, L. M.; Guo, X. F.; Ding, W. P. Catalytic Ammonia Synthesis over Mo Nitride/ZSM-5. *ChemCatChem* **2010**, *2* (2), 167−174.

(25) Azofra, L. M.; Morlanés, N.; Poater, A.; Samantaray, M. K.; Vidjayacoumar, B.; Albahily, K.; Cavallo, L.; Basset, J. M. Single-Site Molybdenum on Solid Support Materials for Catalytic Hydrogenation of N_2-into-NH_3. *Angew. Chem., Int. Ed. Engl.* **2018**, *57* (48), 15812−15816.

(26) Sklenak, S.; Andrikopoulos, P. C.; Boekfa, B.; Jansang, B.; Nováková, J.; Benco, L.; Bucko, T.; Hafner, J.; Dědeček, J.; Sobalík, Z. N_2O Decomposition over Fe-zeolites: Structure of the Active Sites and the Origin of the Distinct Reactivity of Fe-ferrierite, Fe-ZSM-5, and Fe-beta. A Combined Periodic DFT and Multispectral Study. *J. Catal.* **2010**, *272* (2), 262−274.

(27) Tabor, E.; Lemishka, M.; Sobalik, Z.; Mlekodaj, K.; Andrikopoulos, P. C.; Dedecek, J.; Sklenak, S. Low-temperature Selective Oxidation of Methane over Distant Binuclear Cationic Centers in Zeolites. *Commun. Chem.* **2019**, *2* (1), 71.

(28) Tabor, E.; Lemishka, M.; Olszowka, J. E.; Mlekodaj, K.; Dedecek, J.; Andrikopoulos, P. C.; Sklenak, S. Splitting Dioxygen over Distant Binuclear Fe Sites in Zeolites. Effect of the Local Arrangement and Framework Topology. *ACS Catal.* **2021**, *11* (4), 2340−2355.

(29) Baerlocher, C.; McCusker, L. B. *Database of Zeolite Structures*, 2022, http://www.iza-structure.org/databases/.

(30) Shaver, M. P.; Fryzuk, M. D. Activation of Molecular Nitrogen: Coordination, Cleavage and Functionalization of N_2 Mediated By Metal Complexes. *Adv. Synth. Catal.* **2003**, *345* (910), 1061−1076.

(31) Dronskowski, R.; Blöchl, P. E. Crystal Orbital Hamilton Populations (COHP). Energy-Resolved Visualization of Chemical Bonding in Solids Based on Density-Functional Calculations. *J. Phys. Chem.* **1993**, *97* (33), 8617−8624.

(32) Kresse, G.; Furthmüller, J. Efficiency of ab-initio Total Energy Calculations for Metals and Semiconductors Using a Plane-wave Basis Set. *Comput. Mater. Sci.* **1996**, *6*, 15−50.

(33) Perdew, J. P.; Burke, K.; Ernzerhof, M. Generalized Gradient Approximation Made Simple. *Phys. Rev. Lett.* **1996**, *77*, 3865.

(34) Wellendorff, J.; Lundgaard, K. T.; Møgelhøj, A.; Petzold, V.; Landis, D. D.; Nørskov, J. K.; Bligaard, T.; Jacobsen, K. W. Density Functionals for Surface Science: Exchange-correlation Model

https://doi.org/10.1021/jacsau.3c00546
JACS Au 2023, 3, 3374−3380

Development with Bayesian Error Estimation. *Phys. Rev. B* **2012**, *85* (23), 235149.
(35) Brogaard, R. Y.; Moses, P. G.; Nørskov, J. K. Modeling van der Waals Interactions in Zeolites with Periodic DFT: Physisorption of n-Alkanes in ZSM-22. *Catal. Lett.* **2012**, *142* (9), 1057−1060.
(36) Brogaard, R. Y.; Henry, R.; Schuurman, Y.; Medford, A. J.; Moses, P. G.; Beato, P.; Svelle, S.; Nørskov, J. K.; Olsbye, U. Methanol-to-Hydrocarbons Conversion: The Alkene Methylation Pathway. *J. Catal.* **2014**, *314*, 159−169.
(37) Mao, Y.; Wang, H. F.; Hu, P. Theoretical Investigation of NH_3-SCR Processes over Zeolites: A review. *Int. J. Quantum Chem.* **2015**, *115* (10), 618−630.
(38) Henkelman, G.; Uberuaga, B. P.; Jónsson, H. A Climbing Image Nudged Elastic Band Method for Finding Saddle Points and Minimum Energy Paths. *J. Chem. Phys.* **2000**, *113*, 9901−9904.
(39) Medford, A. J.; Shi, C.; Hoffmann, M. J.; Lausche, A. C.; Fitzgibbon, S. R.; Bligaard, T.; Nørskov, J. K. CatMAP: A Software Package for Descriptor-Based Microkinetic Mapping of Catalytic Trends. *Catal. Lett.* **2015**, *145* (3), 794−807.
(40) Benco, L.; Bucko, T.; Grybos, R.; Hafner, J.; Sobalik, Z.; Dedecek, J.; Hrusak, J. Adsorption of NO in Fe^{2+}-exchanged Ferrierite. A Density Functional Theory Study. *J. Phys. Chem. C* **2007**, *111* (2), 586−595.

https://doi.org/10.1021/jacsau.3c00546
JACS Au 2023, 3, 3374−3380